Front. Struct. Civ. Eng. 2021, 15(3): 643–651
https://doi.org/10.1007/s11709-021-0709-9

RESEARCH ARTICLE

Characterization of 3D microstructure, thermal conductivity, and heat flow of cement-based foam using imaging technique

Farnaz BATOOL[a*], Muhammad Saad KHAN[a], Vivek BINDIGANAVILE[b]

[a] *Department of Civil Engineering, NED University of Engineering & Technology, Karachi 75270, Pakistan*

[b] *Department of Civil and Environmental Engineering, University of Alberta, Edmonton T6G2R3, Canada*

[*] *Corresponding author. E-mail: batool1@ualberta.ca*

ABSTRACT This study presents the results of the 3D microstructure, thermal conductivity, and heat flow in cement-based foams and examines their changes with a range of densities. Images were captured using X-ray micro computed tomography (micro-CT) imaging technique on cement-based foam samples prepared with densities of 400, 600, and 800 kg/m^3. These images were later simulated and quantified using 3D data visualization and analysis software. Based on the analysis, the pore volume of 11000 μm^3 was determined across the three densities, leading to optimal results. However, distinct pore diameters of 15 μm for 800 kg/m^3, and 20 μm for 600 and 400 kg/m^3 were found to be optimum. Most of the pores were spherical, with only 10% appearing elongated or fractured. In addition, a difference of 15% was observed between the 2D and 3D porosity results. Moreover, a difference of 5% was noticed between the experimentally measured thermal conductivity and the numerically predicted value and this variation was constant across the three cast densities. The 3D model showed that heat flows through the cement paste solids and with an increase in porosity this flow reduces.

KEYWORDS 3D pore volume distribution, X-ray tomography, 3D shape factor, heat flow

1 Introduction

Population growth and energy crises have increased the demand for energy-efficient and low-cost housing. The global construction industry is searching for sustainable building materials that meet these requirements. In this context, cement-based foam (also called foamed concrete or cellular concrete), which is a lightweight material, offers numerous advantages owing to its ease of compaction, good insulation, and low density. In addition, the use of agricultural/industrial waste as supplementary cementing admixtures further boosts both economic and environmental costs. Cement-based foam is a mixture of Portland cement, water, and preformed foam added to create an air-void network [1]; lower densities are primarily designed as aerated paste, while higher densities may sometimes comprise fine aggregates [1].

The microstructure and air-void network within cement-based foams influence their physical, mechanical, and thermal properties [2–6]. Prior research has mostly employed 2D image analysis techniques such as optical microscopy and scanning electron microscopy (SEM) to characterize the pore structure parameters [7–10]. For instance, Nambiar and Ramamurthy [7] used optical microscopy and observed a wider distribution of air voids and lower strength for higher foam volume. A similar procedure was adopted by Wee et al. [8] for lightweight foamed concrete microstructure analysis. They concluded that there is an inverse relationship between pore spacing and porosity. Using a scanning electron microscope SEM, Hilal et al. [9] observed larger irregular voids and wider distribution sizes in the pore structure of cement-based foams that contain more foam. This study also reported an improvement in strength with a reduction in pore size.

Recent advancements in X-ray tomography techniques have provided a new direction for the microstructural characterization of cementitious materials [10–13]. X-ray tomography is a three-dimensional imaging technique that measures the internal structure of a material through X-ray

Article history: Received May 17, 2020; Accepted Jul 11, 2020

absorption [12] without altering the internal microstructure details. This alteration was common in earlier 2D imaging methods, which are usually performed during sample preparation. In a recent study, the authors used an X-ray tomography technique to quantify the pore structure and found smaller pores governing thermal conductivity [12]. Using a similar method, Chung et al. [13] found that the pore size decreased with an increase in the cast density. Prior research has endeavored to simulate the thermal conductivity, heat flow, and mechanical properties through analysis of resulting 3D X-ray tomography images [3,13,14]. These authors used a regenerated 3D microstructure to model cement-based foam for further analysis. However, such numerical models can only capture undisturbed pores accurately, excluding those that are broken or merged. This emphasizes the evaluation of the hardened properties of cement-based foam via 3D modeling with all types of pores included, which is yet to be explored.

The present study investigates the 3D microstructure of cement-based foams and correlates the parameters of the air-void network with those of the thermal conductivity and heat flow. Using the 3D model generated through X-ray micro computed tomography (micro-CT) images, the quantified parameters were compared with the density (800–400 kg/m^3), porosity, and foam volume. The results are expected to enable future manufacturers to extend the applications of cement-based foam as an insulating material.

2 Material and methods

2.1 Mix proportions

Cement-based foam samples were cast with three densities: 800, 600, and 400 kg/m^3. Here, the slurry for the mixtures was prepared using Type HE Portland cement (Table 1) conforming to CAN/CSA A3000 [15], while the pore structure was created using a synthetic foaming agent [16]. The details of the mixtures with other mix proportions are listed in Table 2.

Table 1 Chemical and physical properties of cement.

component	cement (%)
SiO_2	21
Fe_2O_3	4.4
Al_2O_3	4
CaO	62
MgO	3.34
SO_3	2.08
unit density (kg/m^3)	3, 120
particle size (μm)	10–15
specific surface area (m^2/kg)	406

2.2 Specimens

The cement-based foam specimens were prepared in two stages. In the first stage, the slurry and preformed foam were prepared separately. In the second stage, the preformed foam was gradually added to the slurry, prepared by mixing water with cement to achieve the desired cast density. The preformed foam was prepared by aerating the foam solution through a mini (12 mm) open-air foam generating system activated using compressed air at the pressure of 0.70 MPa. This foam solution, which resulted in a foam density of 40 kg/m^3, was prepared by mixing 3% of the foaming agent with water. The mixing and addition of foam into slurry requires intermittent checking of the composite density, which was performed with the help of a container. Upon reaching the desired cast density, the mixture was poured into molds, each with the height of 150 mm and diameter of 75 mm. The samples were stored in a curing room for 28 d and thereafter, left to dry in air. From these cylinders, three specimens of size 35 mm × 35 mm × 20 mm having different densities were obtained for X-ray tomography. All scans were performed at 300 d of maturity.

2.3 Test method

In this study, a Skyscan 1076 micro-computed X-ray tomography (μCT) machine was used to scan the cement-based foam samples, capturing images at the resolution of 9 μm. Subsequently, these raw images were reconstructed to enable detection of the details using the NRecon software. Thereafter, the Xlab module of a high-performance 3D imaging and analysis solution software, Avizo version 9.0.1, was used for the 3D simulation and quantitative analysis. The Xlab module applies a finite volume method to solve the equation systems and discretize the model into isotropic cubic voxels. Here, the selected sample was divided into voxel sizes of 1 μm × 1 μm × 1 μm with macroscopic boundary conditions. This boundary condition is the constant temperature at the two opposite faces, while the inter-phase boundary conditions were set such that the temperature and heat flux remained continuous at the interface of the two phases. A data set of 100 reconstructed or gray images was selected and processed using the software by defining a rectangular region of interest, as shown in Fig. 1.

Using this software, various parameters were quantified, including 3D porosity, surface area, and shape factor, after duly thresholding the image to distinguish between the solid and void phases. The XLab module was then utilized to evaluate the thermal conductivity based on the difference in the temperature of the surface area (298K–338K), with the thermal conductivities of the air (0.0257 $W \cdot m^{-1} \cdot K^{-1}$) and solid cement paste (0.458 $W \cdot m^{-1} \cdot K^{-1}$) [17] as input. In this study, three samples for each cast density were quantified. During the analysis

Table 2 Mix proportions of cement-based foam.

substitution type/mix ID	mixture proportion				
	required cast density (kg/m^3)	cement (kg/m^3)	water (kg/m^3)	foam volume (%)	water/binder ratio
plain (PN)	800	474	327	43	0.69
	600	355	245	58	
	400	237	164	76	

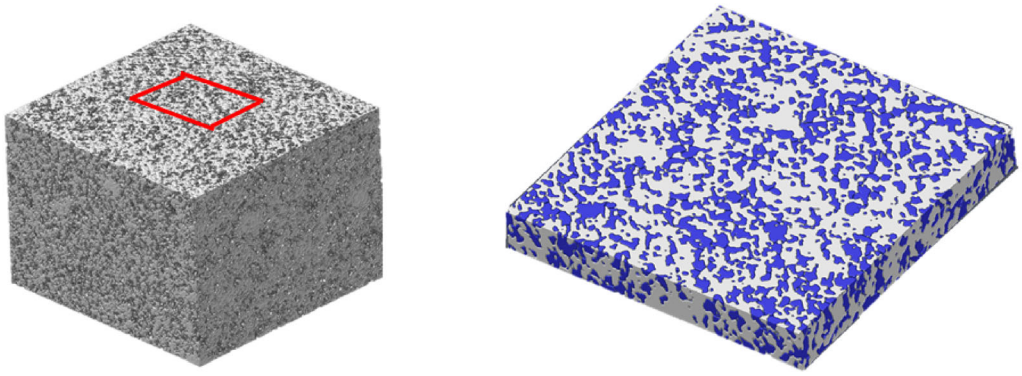

(a) (b)

Fig. 1 (a) Micro-CT images of 3D cement-based foam sample; (b) pore structure of cement-based foam after rendering (blue portion shows pores within the matrix and white shows the cement paste).

process, the calibration of pore parameters was carried out using the thermal conductivity data reported in Ref. [5], measured experimentally on cement-based foam samples.

3 Results and discussion

3.1 3D porosity and foam volume

Figure 2 presents the scanning electron microscopy SEM micrographs of the cement-based foam microstructure. As shown in the figure, the microstructure includes pores, created deliberately by adding preformed foam and a pore wall of solid hydrated cement paste. As the density decreased, the number of pores increased, and the wall size decreased. This indicates that the changes in the micro-structural parameters are associated with the density. The 3D pore structures shown in Fig. 3 further elaborate on this association with the change in pore size and the number of pores. As the density decreased, the pores became larger. It can be noticed from Fig. 3(a) that pores with diameters of 0–25 μm are more in number than pores with sizes of 25–40 μm. However, Figs. 3(b) and 3(c) show the formation of larger pore sizes. This formation primarily depends on the foam volume, which plays a vital role in achieving the required density. Figure 4 further clarifies this relationship and demonstrates that a higher foam volume results in a lower density. Therefore, it can be anticipated that a slight variation in foam volume will significantly change the density as well as the pore structure. It should be mentioned here that the porosity includes only those pores that were created as a result of the preformed foam; as expected, the lower the density, the higher the porosity. In comparison with the foam volume, the 3D porosity was uniformly lower by approximately 7%. This is likely because some of the foam bubbles either break or merge during the handling and mixing process. The present authors have previously reported the 2D porosity of the same mixtures [12]. It is seen that the 3D measurements uniformly result in 15% lower values compared with the 2D measurements.

Figure 5 further explains the porosity through a plot of the relationship of the average pore volume and density of cement-based foam against the foam volume. It is seen that pore volume increases with the addition of foam. When related with density, these larger pore volumes were found to occur in lower density foam, i.e., 400 kg/m^3, while those with higher densities had small pore volume formation in comparison. Moreover, with the reduction in density from 800 to 600 and then to 400 kg/m^3, the pore volume increased by 45% in the mixtures. This difference is quite significant but was expected as the volume of foam is inversely related to density.

3.2 3D pore size parameters and influence on density

The pore volume of 11000 μm^3 was determined to be the optimum for all mixtures, and this can be observed from the frequency histograms of the pore volume distribution presented in Fig. 6. For this pore volume, the maximum

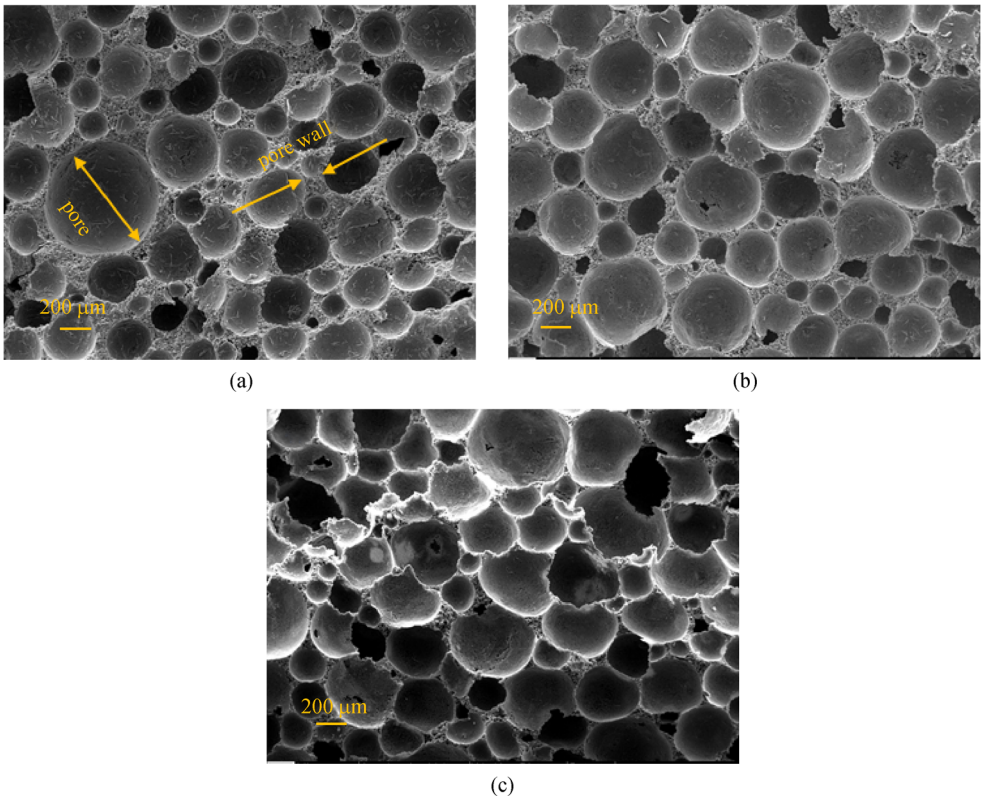

Fig. 2 SEM images of cement-based foam mixtures: (a) 800 kg/m^3; (b) 600 kg/m^3; (c) 400 kg/m^3.

occurrence recorded was for the 400 kg/m^3 mixture. Furthermore, it can be observed that the incidence of the pore volume having smaller size is high for 800 kg/m^3, while the densities of 600 and 400 kg/m^3 exhibit larger pore volumes. This implies that the formation of larger pore volume sizes increases as the density reduces, shown by the results in Figs. 2 and 3, which strengthens the credibility of these findings. In addition, the overlapping and merging of bubbles during the mixing process could be a reason for the formation of a larger pore volume. Another parameter that further explains the pore size is the equivalent diameter, as illustrated in Fig. 7. It can be observed that the pore diameter of 15 μm is optimum for 800 kg/m^3; whereas, for 600 and 400 kg/m^3, the pore size of 20 μm predominates. Accordingly, the 800 and 600 kg/m^3 mixture frequencies were found to be higher for pore diameters in the range of 5–15 μm, and the frequency gradually decreased at 20–60 μm. For 400 kg/m^3, the trend differed as a gradual increase in the frequency of occurrence was observed. This implies that the micro-structures of higher densities comprise small pores compared with those of lower densities.

3.3 3D shape factor and influence on density

The pore shape distribution may be well-characterized using the aspect ratio and shape factor of the average pore [18]. An aspect ratio of unity implies a perfect spherical shape, while values greater than one represent fractured or elongated pores [18]. Figure 8 displays plots of the results for the aspect ratio of the cement-based foam mixtures across the three densities. Here, the aspect ratio was calculated by dividing the 3D pore length by the 3D pore width. It can be seen that across the three densities, approximately 11%, 6%, and 4% of pores have an aspect ratio greater than unity at 800, 600, and 400 kg/m^3, respectively. On the other hand, at least 60% of the pores may be said to be spherical for all densities. Therefore, most of the pores were spherical, and 10% could be elongated or fractured. These findings are supported by the results of the shape factor presented in Fig. 9, which shows that 85% of the pores are between 1 and 5 (across all densities). Additionally, for a density of 800 kg/m^3, 15% of the pores were found to be spherical, which is high in comparison with other densities (Fig. 9). This percentage is not surprising as, at higher densities, the cement-based foam constitutes more paste and fewer pores. As evidence, the SEM results shown in Fig. 2 may be revisited here. In addition, from Fig. 2(a), it can be noticed that the pores at a density of 800 kg/m^3 appear more stable and well-defined compared with those at lower densities.

3.4 Numerical prediction of thermal conductivity

The numerically simulated thermal conductivity results obtained using the 3D model for cement-based foam

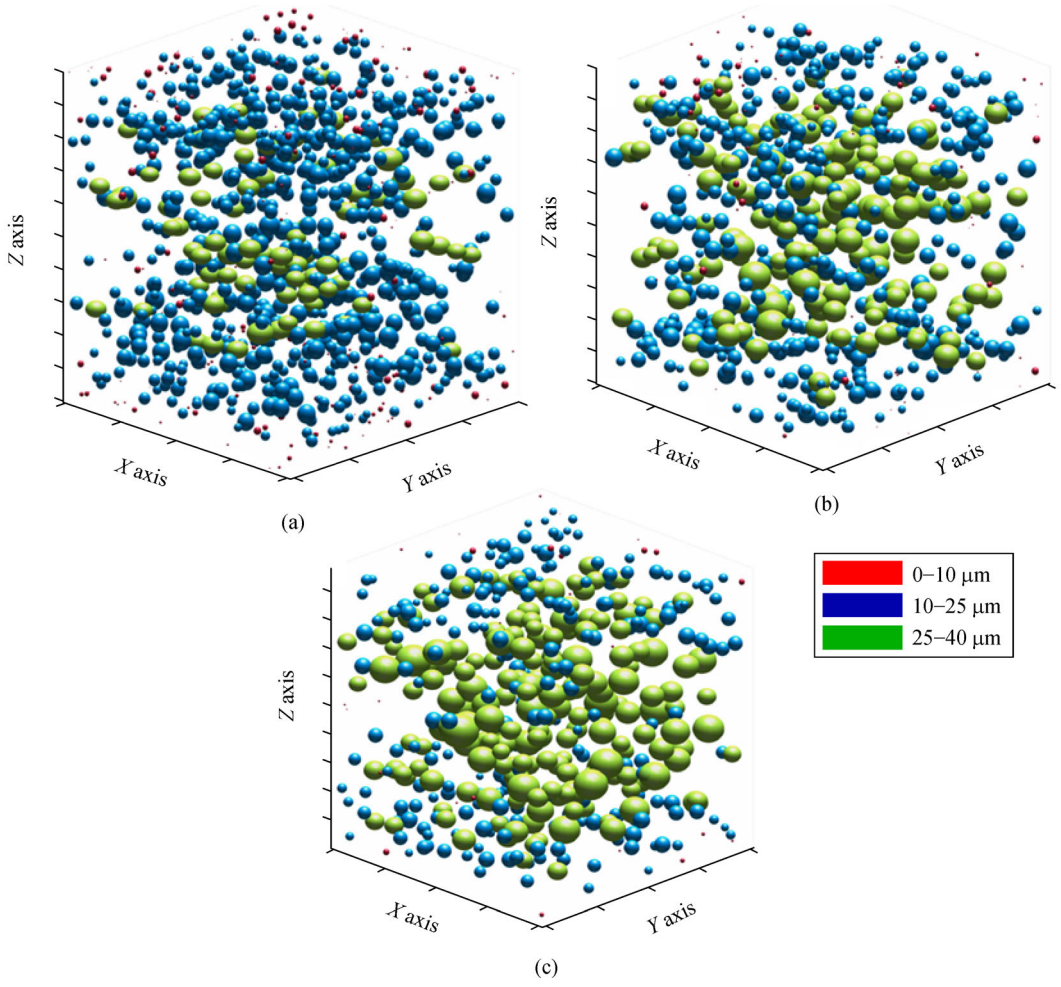

Fig. 3 3D microstructures of cement-based foam mixtures: (a) 800 kg/m^3; (b) 600 kg/m^3; (c) 400 kg/m^3.

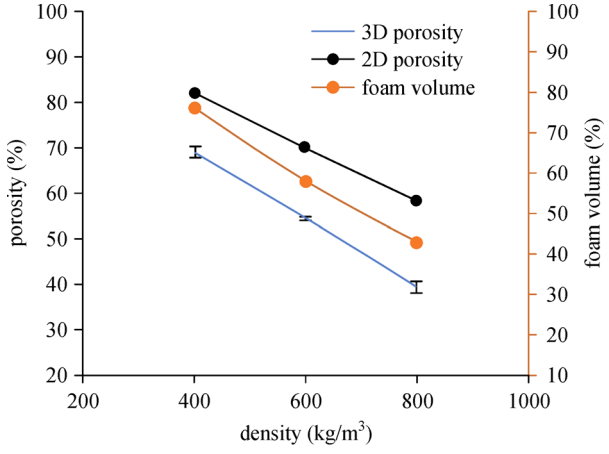

Fig. 4 Relationship between 3D porosity, density, and foam volume (with standard error mean bar).

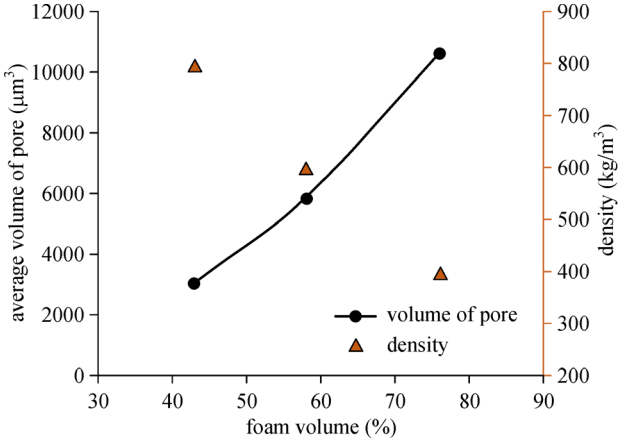

Fig. 5 Relationship between the volume of pores and foam volume for cement-based foam mixtures.

mixtures are presented in Fig. 10. It can be observed that the thermal conductivity is directly related to the density of the cement-based foam. This finding was expected because as the density decreases, the cement matrix reduces and the number of pores increases, thus decreasing the conductivity. In addition, Fig. 11 presents a comparison of the

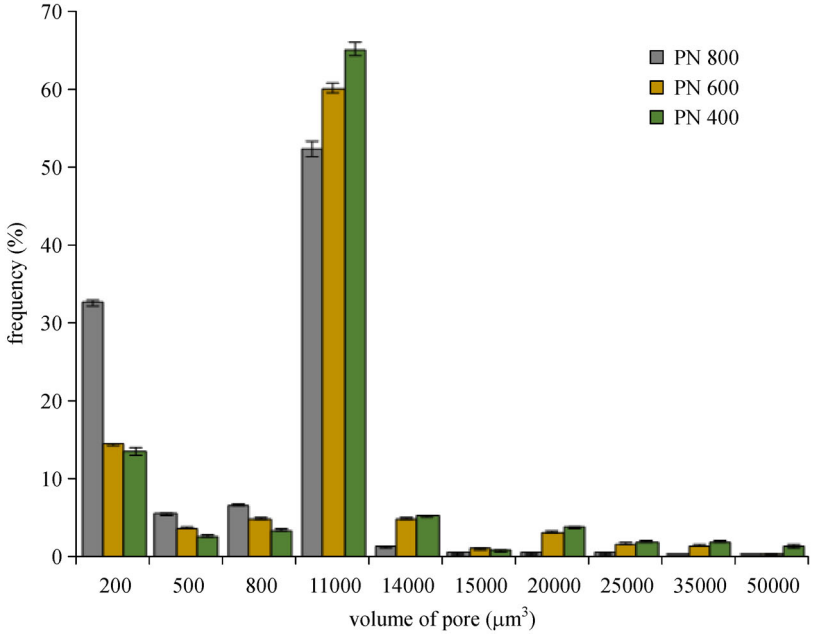

Fig. 6 Pore volume distribution for cement-based foam mixtures (with standard error mean bar).

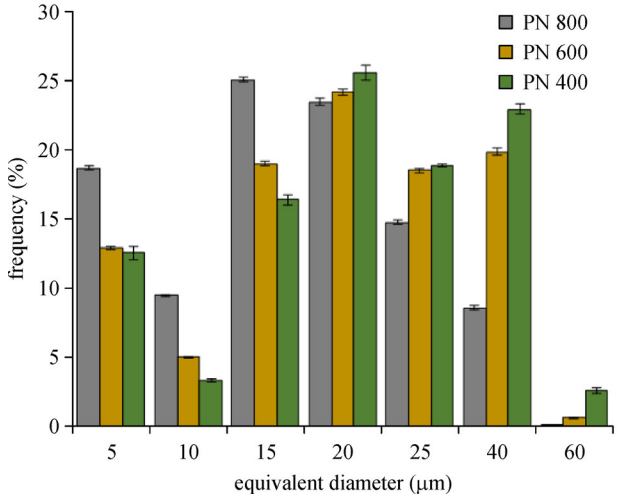

Fig. 7 Pore diameter distribution for cement-based foam mixtures (with standard error mean bar).

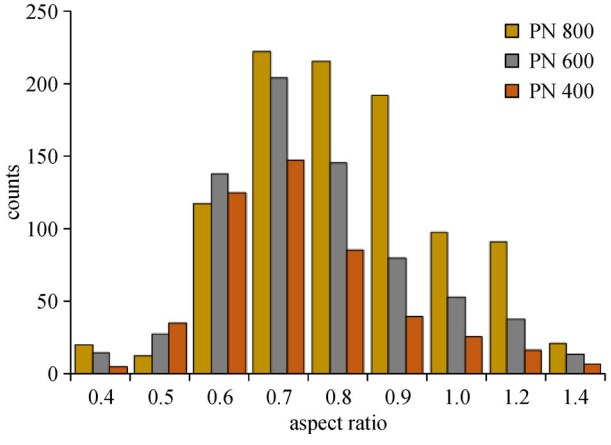

Fig. 8 Aspect ratio for cement-based foam mixtures.

simulated thermal conductivity results of cement-based foam mixtures with those experimentally measured. These predicted values agree with the experimental evaluation obtained from an earlier report [5]. This experimental evaluation was conducted by the same authors in a separate study [5]. The thermal conductivity of the cement-based foam was slightly underestimated for the mixtures with higher densities, and the percentage error reported between the numerical and observed values was 5% for 800 kg/m^3 and 4% for the two remaining densities. This difference is primarily due to the threshold values selected during the binary process.

3.5 Influence of D50 and D90 on thermal conductivity

From Fig. 12, the relationship between the thermal conductivity and the pore volume parameters D50 and D90 can be studied. The pore sizes, D50 and D90, are specifically the pore volume sizes that occur below 50% (median) and 90%, respectively, of the entire set of pores. These parameters were evaluated by plotting the cumulative frequency distribution of the pore sizes, as presented in Fig. 6. Additionally, a detailed analysis of D50 and D90 can be found in Ref. [12]. As shown in Figs. 12(a) and 12(b), the thermal conductivity was found to be inversely related to D50 and D90. With a lower value of D50, pore volume sizes resulted in higher thermal conductivity, which was found in the mixture of 800 kg/m^3. However,

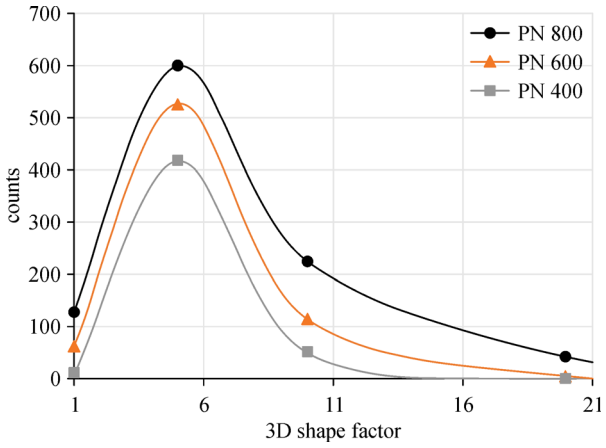

Fig. 9 Shape factor for cement-based foam mixtures.

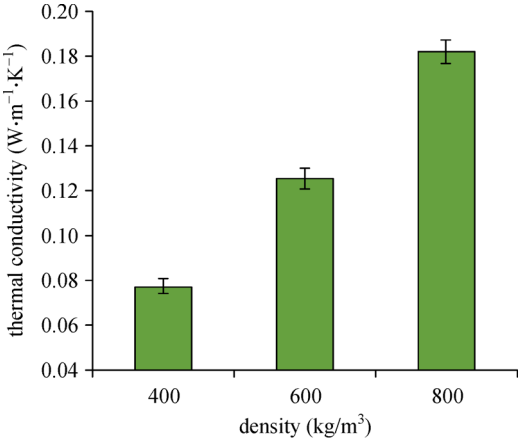

Fig. 10 Relationship between thermal conductivity and density (with standard error mean bar).

for the mixtures of 600 and 400 kg/m^3, higher D50 values caused lower conductivity. This implies that a larger pore

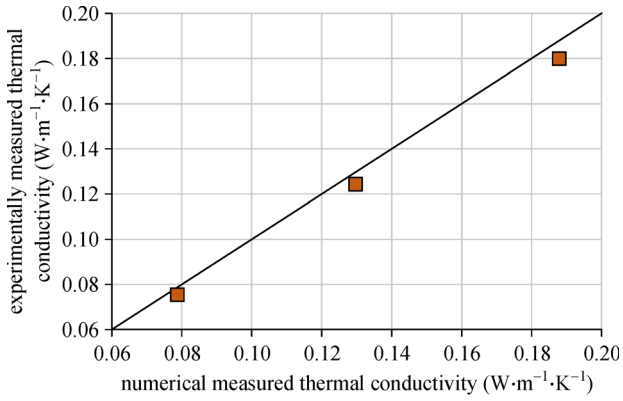

Fig. 11 Comparison between numerical and experimentally measured thermal conductivity results.

volume reduces conductivity. These results support the experimental findings presented earlier [12], wherein smaller pore diameters resulted in higher thermal conductivity.

3.6 Heat flow in cement-based foam

Figures 13–15 illustrate the temperature distribution and heat flow for cement-based foam mixtures across the three cast densities. As shown, the pore wall, which constitutes cement paste, forms a continuous conduction pathway. She et al. [3] reported that heat transfer in foamed concrete is primarily due to conduction, as other mechanisms such as convection and radiation are negligible due to smaller pore diameters. In Figs. 13(a), 14(a), and 15(a), the number of pathways was found to decrease with an increase in porosity or with a reduction in density. A separate illustration of heat vectors in Figs. 13(b), 14(b), and 15(b) shows the flow of heat through the cement paste in the walls while evading the pores. The difference in the thermal conductivity of the two phases is likely the reason

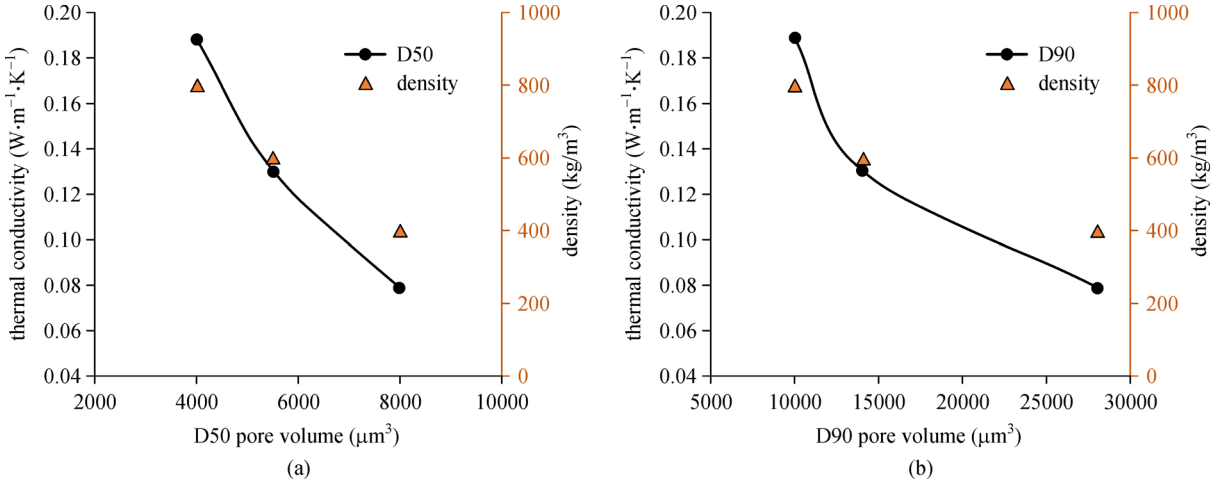

Fig. 12 Relationship of thermal conductivity with pore volume parameters: (a) D50; (b) D90.

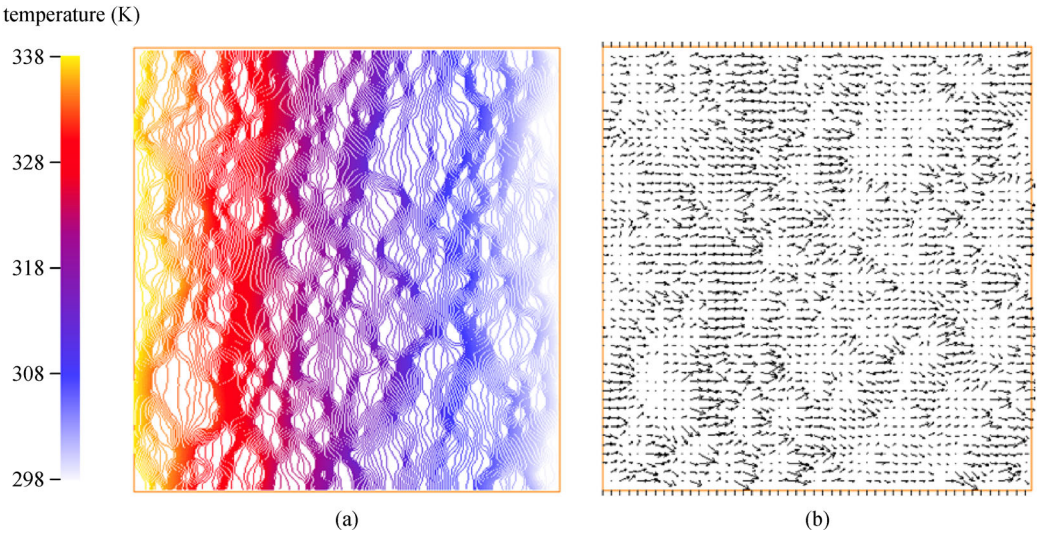

Fig. 13 Cement-based foam mixture with density of 800 kg/m^3: (a) temperature distribution; (b) heat flow.

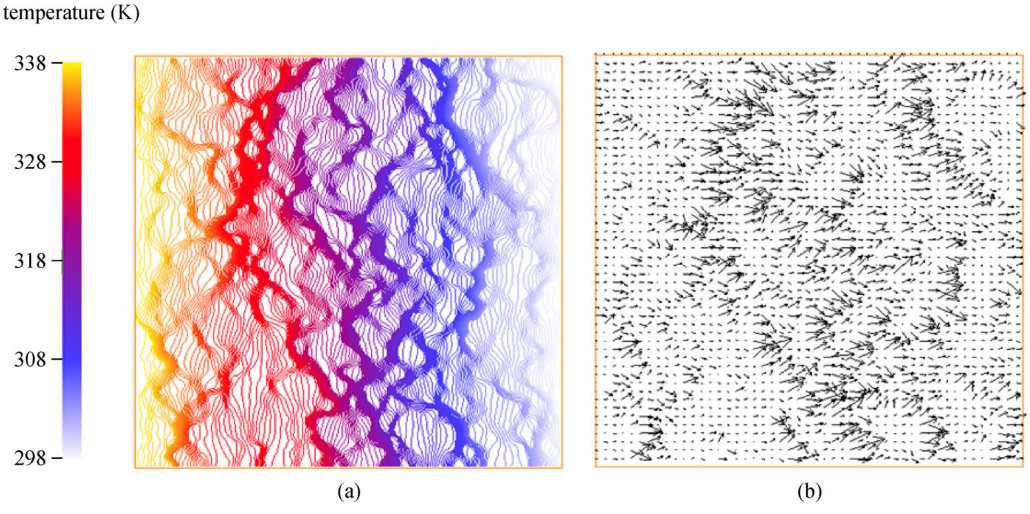

Fig. 14 Cement-based foam mixture with density of 600 kg/m^3: (a) temperature distribution; (b) heat flow.

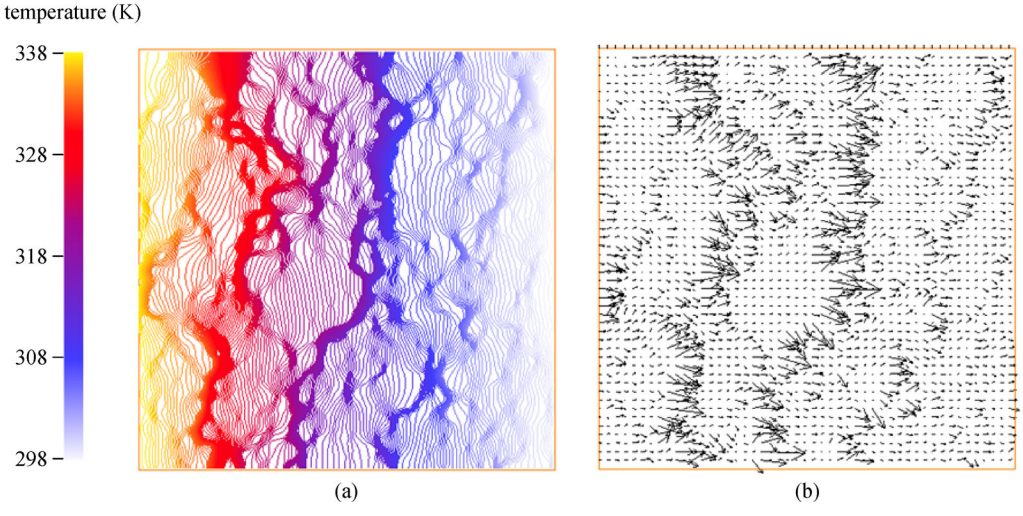

Fig. 15 Cement-based foam mixture with density of 400 kg/m^3: (a) temperature distribution; (b) heat flow.

for this. Additionally, a smooth heat flow pattern can be observed for lower porosity (800 kg/m^3); however, as the porosity increases and the density decreases, the flow becomes irregular, with heat vectors converging around the pores. Similar findings were reported by Carson et al. [19] while investigating porous granular materials and She et al. [3] in the evaluation of thermal properties of cement-based foam. This implies that heat is transferred through those phases that have higher thermal conductivity and, in cement-based foams, the medium is the hydrated cement paste in the walls.

4 Conclusions

In this study, the 3D microstructural parameters of cement-based foam were quantified using X-ray tomography technique. Their influence on the thermal conductivity and heat flow was established for the density range of 800–400 kg/m^3. Based on these findings, the following conclusions can be drawn.

1) An increase in the volume of the preformed foam leads to higher porosity, and a difference of almost 7% was recorded between this volume and the 3D porosity at a given density. The 3D porosity was about 15% lower than that measured using 2D imaging.

2) The pore volume of 11000 μm^3 was found to be the optimum for all mixtures. While pore diameters of 15 μm was optimal for 800 kg/m^3, and 20 μm for 600 and 400 kg/m^3, respectively.

3) The microstructure of cement-based foams at higher densities comprises smaller pore diameters compared with those at lower densities. Most of the pores were found to be spherical, while about 10% were elongated or fractured pores.

4) The numerical and experimental results for the thermal conductivity of cement-based foam were found to be similar with a percentage error of approximately 5% for the three densities.

5) The D50 and D90 pore size parameters inversely correlate with the thermal conductivity and density.

6) The heat flow pathway formed through the cement paste (pore wall), avoiding the pores, and an increase in porosity was found to reduce this pathway.

Acknowledgements The authors thank the NED University of Engineering and Technology for providing the simulation facilities. We also thank the Natural Sciences and Engineering Research Council NSERC-Canada for providing funding.

References

1. Amran Y, Farzadnia N, Abang Ali A. Properties and applications of foamed concrete: A review. Construction & Building Materials, 2015, 101: 990–1005
2. Awang H, Mydin M A O, Roslan A F. Effect of additives on mechanical and thermal properties of lightweight foamed concrete. Pelagia Research Library Advances in Applied Science Research, 2012, 3: 3326–3338
3. She W, Chen Y, Zhang Y, Jones M. Characterization and simulation of microstructure and thermal properties of foamed concrete. Construction & Building Materials, 2013, 47: 1278–1291
4. Samson G, Phelipot-Mardelé A, Lanos C. Thermal and mechanical properties of gypsum–cement foam concrete: effects of surfactant. European Journal of Environmental and Civil Engineering, 2016, 21(12): 1–20
5. Batool F, Bindiganavile V. Quantification of factors influencing the thermal conductivity of cement-based foam. Cement and Concrete Composites, 2018, 91: 76–86
6. Falliano D, de Domenico D, Ricciardi G, Gugliandolo E. Improving the flexural capacity of extrudable foamed concrete with glass-fiber bi-directional grid reinforcement: An experimental study. Composite Structures, 2019, 209: 45–59
7. Nambiar E, Ramamurthy K. Air-void characterisation of foam concrete. Cement and Concrete Research, 2007, 37(2): 221–230
8. Wee T, Tamilselvan T, Lim H, Babu D. Air-void system of foamed concrete and its effect on mechanical properties. ACI Materials Journal, 2006, 103(1): 45–52
9. Hilal A, Thom N, Dawson A. On void structure and strength of foamed concrete made without/with additives. Construction & Building Materials, 2015, 85: 157–164
10. Bentz D, Quenard D, Kunzel H, Baruchel J, Peyrin F, Martys N, Garboczi E J. Microstructure and transport properties of porous building materials. II: Three-dimensional X-ray tomographic studies. Materials and Structures, 2000, 33(3): 147–153
11. Nguyen T, Ghazlan A, Kashani A, Bordas S, Ngo T. 3D meso-scale modelling of foamed concrete based on X-ray computed tomography. Construction & Building Materials, 2018, 188: 583–598
12. Batool F, Bindiganavile V. Air-void size distribution of cement-based foam and its effect on thermal conductivity. Construction & Building Materials, 2017, 149: 17–28
13. Chung S, Lehmann C, Abd Elrahman M, Stephan D. Pore characteristics and their effects on the material properties of foamed concrete evaluated using micro-CT images and numerical approaches. Applied Sciences (Basel, Switzerland), 2017, 7(6): 550
14. She W, Zhang Y, Jones M. Three-dimensional numerical modeling and simulation of the thermal properties of foamed concrete. Construction & Building Materials, 2014, 50: 421–431
15. CAN/CSA A3000. Cementitious Materials Compendium, Canadian Standards. Ontario: Association Mississauga, 2013
16. ASTM C869. Standard Specification for Foaming Agents Used in Making Preformed Foam for Cellular Concrete. West Conshohocken, PA: ASTM International, 2012
17. Batool F, Bindiganavile V. Thermal conductivity of hydrated paste in cement-based foam microstructure. Advances in Civil Engineering Materials, 2018, 7(1): 17–32
18. Kong L, Ostadhassan M, Li C, Tamimi N. Pore characterization of 3D-printed gypsum rocks: A comprehensive approach. Journal of Materials Science, 2018, 53(7): 5063–5078
19. Carson J, Lovatt S, Tanner D, Cleland A. Thermal conductivity bounds for isotropic, porous materials. International Journal of Heat and Mass Transfer, 2005, 48(11): 2150–2158